Available online at www.sciencedirect.com
ScienceDirect
International Journal of Heat and Mass Transfer 50 (2007) 847–856
International Journal of HEAT and MASS TRANSFER
www.elsevier.com/locate/ijhmt

An iterative stabilized CNBS–CG scheme for incompressible non-isothermal non-Newtonian fluid flow

Xianhong Han, Xikui Li *

State Key Laboratory of Structural Analysis of Industrial Equipment, Dalian University of Technology, Dalian 116023, PR China

Received 5 December 2005; received in revised form 21 August 2006
Available online 7 November 2006

Abstract

An iterative stabilized fractional step scheme abbreviated as I-CNBS–CG is developed, in which the Crank–Nicolson method based split (CNBS) scheme and the characteristic-Galerkin (CG) method are, respectively, used to discretize and solve the non-Newtonian momentum–mass conservation equations and the energy conservation equation in consideration of their convective character. Owing to introduction of an iterative procedure into the scheme the stability of the proposed scheme in time domain is greatly enhanced and much larger time step sizes are allowed to be used than those limited in existing explicit and semi-implicit ones. The proposed I-CNBS–CG scheme particularly suits to numerically model the non-isothermal non-Newtonian fluid flows with moderate or high viscosity and low thermal conductivity, such as molten polymer flow process in a mould cavity. Numerical experiments with the power-law fluid model demonstrate the improved performances of the proposed scheme.

Keywords: Incompressible non-isothermal non-Newtonian fluid; Finite element method; Fractional step algorithm; Iterative procedure; Crank–Nicolson method; Characteristic-Galerkin method

1. Introduction

Fractional step algorithms have enjoyed widespread popularity since the original works of Chorin [1] and Temam [2] for incompressible flow problems. One of the main reasons for this popularity relies on the computational efficiency of the algorithms [3], mainly owing to uncoupling of the pressure term from the velocity components. On the other hand, the algorithms were used as a stabilization technique to circumvent the LBB restrictions (also referred to the inf-sup condition, which precludes the use of elements with equal low order interpolations for velocities and pressure, unless special stabilization techniques are used) though recent studies [4,5] indicate that this bonus is not available for all types of fractional step schemes, nevertheless that is not the focus of this paper, and indeed only those elements satisfying the LBB condition are used in this paper.

The explicit (or semi-explicit) form of the algorithm is popular and widely employed in practical engineering computations since its simplicity in programming and economy in computational efforts required for each time step, but at the expense of conditional stability, which implies that the time steps will be inevitably small and a restriction in maximum time step size is imposed to the algorithm. Particularly in modeling high-viscosity (low Reynolds number) fluid flows such as molten polymer flow in injection molding, the maximum time step size allowed for the explicit form of the algorithm decreases with increasing viscosity that reduces the efficiency of the numerical solution procedure. Though the limitation in the maximum time step size to the explicit form of the algorithm can be alleviated in the semi-explicit form to some extent, numerical results of test examples [6] indicate that the limitation still restricts applications of the algorithm with acceptable efficiency and accuracy.

* Corresponding author. Tel./fax: +86 411 84709186.
E-mail address: xikuili@dlut.edu.cn (X. Li).

0017-9310/$ - see front matter © 2006 Elsevier Ltd. All rights reserved.
doi:10.1016/j.ijheatmasstransfer.2006.08.037

Nomenclature

c	heat capacity
$\mathbf{D}_0$	a constant matrix equal to diag(2 2 2 1 1 1)
D_{ij}	rate of strain tensor
$\mathbf{g}$	body force
$h(\Delta\mathbf{u})$	higher-order differential
$\mathbf{I}_3$	the 3×3 identity matrix
k	thermal conductivity
m	consistency coefficient
n	power law index
$\mathbf{N}_u$	finite element shape functions for velocity ($\mathbf{N}_p$, $\mathbf{N}_T$ for pressure and temperature)
p	pressure
Pe	thermal Peclet number
$\mathbf{S}$	operator matrix
t	time
Δt	time step size
$\Delta t_{\max}$	maximum time step size
T	temperature
T_0	temperature along the solid wall boundary
T_{ref}	reference temperature
T_{entry}	temperature at the inlet
u_i	velocity component in i-direction ($i = 1, 2, 3$)
u_i^*	auxiliary velocities
x, y	horizontal and vertical coordinates
X_0, Y_0	length and height of the cavity

Greek symbols

α	coefficient to normalize the fluid flux equal to unit at the entry
β	temperature dependent coefficient
$\dot{\gamma}$	rate of equivalent strain
$\dot{\gamma}_0$	a constant rate of equivalent strain (10^{-4})
η	L^2 norm of the relative error
θ	time discretization choice
λ	a material time constant
μ	non-Newtonian viscosity
ρ	fluid density
ϕ	thermal dissipation function
Γ	boundary

Superscript

-(overbar) nodal values

Two modified schemes of the fractional step algorithm have been proposed for finite element solutions of incompressible N–S equations [6]. They are based on introducing an iterative procedure into the algorithm to make both the diffusive and convective terms satisfy the momentum conservation equation in an implicit sense. Other schemes for introducing the iterative procedure into the fractional step algorithm can be found in [7,8]. The proposed iterative schemes allow much larger time step sizes to be used for the numerical solutions of incompressible N–S equations with different values of the Reynolds number ranging from low to high viscosities.

The numerical simulation of non-Newtonian fluid flow has attracted increasing attentions due to its comprehensive applications to engineering practices such as chemical process industries, food and construction engineering, petroleum production, bioengineering, etc [9–14]. As compared with the numerical solution procedure for the Newtonian fluid flow governed by incompressible N–S equations, non-linearity of the solution procedure for the non-Newtonian fluid flow stems from not only the convective term in the momentum equation but also the variation of its viscosity with respect to strain rates depending on distributions of the primary variables, i.e. the velocities and the pressure, to be determined. In this view point to introduce the iterative process into the scheme is rather logical and especially desired to ensure the satisfaction of the non-linear momentum conservation with acceptable accuracy and efficiency.

In this paper, the iterative scheme of the fractional step algorithm abbreviated as I-CNBS scheme presented in [6] is extended to simulate the non-Newtonian fluid flow coupled with non-isothermal field. (This scheme was presented as Taylor–Galerkin like based split method in [6], while after a sophisticated consideration, it may be more appropriate to classify the scheme as a Crank–Nicolson method based split one, upon which it is named as I-CNBS scheme in this paper.)

The solution procedure for non-isothermal non-Newtonian fluid flows is further complicated since the additional non-linearity arising from the dependence of the fluid viscosity on temperature and the influence of the velocity–pressure field of the fluid flows on the temperature distribution, particularly for the convection dominated flow problems.

The energy conservation equation to govern the temperature field of fluid flows and its evolution with respect to time can be written in terms of the temperature variable for incompressible flow computations. The energy conservation equation is identical in the form to scalar convection-diffusion equation. As the standard finite element interpolation approximation is not valid for convection-diffusion equations with the character of non-self-adjoint operator a stabilized method is required to develop for the discretization of the energy conservation equation. In the present work, the energy conservation equation is discretized in spatial domain using the characteristic-Galerkin (CG) method.

Due to the coupled effects between the velocity–pressure field and the temperature field, a simultaneous solution procedure for nodal velocities, nodal pressures and nodal temperatures, as primary variables, is generally required

in principle. However, the coupling of the energy conservation equation with the momentum and mass conservation equations is rather weak in incompressible flows, the energy conservation equation can be discretized and solved separately from the discretization and solution procedure for the momentum and mass conservation equations in a staggered solution strategy, particularly in view of computational efficiency and the structure of existing fractional step algorithm for the velocity–pressure solution procedure.

Indeed an iterative procedure for incompressible non-isothermal non-Newtonian fluid flows abbreviated as I-CNBS–CG is constructed so that a staggered solution scheme is particularly designed to solve the velocity–pressure variables by using CNBS scheme for the momentum and the mass conservation equations and to solve the temperature variables by using CG method for the energy conservation equation. The iterative process is performed over both CNBS and CG solution procedures. It is remarked that the proposed I-CNBS–CG scheme is particularly suitable for such a solution strategy in its solution frame and beneficial to accuracy and efficiency of the solution procedure.

The theoretical analysis in the truncation error and stability for the numerical simulation of Newtonian fluid flow by using the proposed I-CNBS scheme has been carried out [15]. However, its extension to non-Newtonian fluid flow is not straightforward, instead, is considerably difficult to tackle. One of the main reasons for this is that the discretized momentum equation (9) in non-Newtonian fluid flow is no longer equivalent to its split form of Eqs. (10) and (11). In fact, an approximation to the diffusive term of Eq. (9) is introduced in the splitting procedure, therefore, the truncation error analysis for Eqs. (10) and (11) cannot simply proceed with the analysis for Eq. (9). In addition, the diffusive term is no longer able to be expressed as the second order derivative of the velocity due to the variable viscosity and consequently the von Newman method in common use for the stability analysis does not apply any more and some more sophisticated method for the stability analysis is required. Indeed in this paper, the improved performance of the scheme is demonstrated with the numerical results for the particular examples, i.e. plan Poiseuille flow problem for isothermal case and 4:1 contraction flow problem for non-isothermal case, given in the Section 3.

2. Governing equations and the iterative fractional step scheme for non-isothermal non-Newtonian fluid flows

Momentum, mass and energy conservation equations for incompressible flows can be written in the matrix-vector form as

$$\rho \mathbf{u}_t + \rho \mathbf{u}\cdot\nabla\mathbf{u} = \rho\mathbf{g} + \mathbf{S}^{\mathrm{T}}(\mu\mathbf{D}_0\mathbf{S})\mathbf{u} - \nabla\cdot(p\mathbf{I}_3) \tag{1}$$

$$\nabla\cdot\mathbf{u} = 0 \tag{2}$$

$$\rho c T_t + \rho c\mathbf{u}\cdot\nabla T = \nabla\cdot(k\nabla T) + \phi \tag{3}$$

where the velocities u_i, the pressure p and the temperature T are the primitive independent variables. ρ is the fluid density, $\mathbf{g} = [g_1 g_2 g_3]$ the body forces, $\mathbf{D}_0 = \mathrm{diag}(2\,2\,2\,1\,1\,1)$, $\mathbf{I}_3$ the 3×3 identity matrix and operator matrix $\mathbf{S}$

$$\mathbf{S}^{\mathrm{T}} = \begin{bmatrix} \partial/\partial x_1 & 0 & 0 & \partial/\partial x_2 & 0 & \partial/\partial x_3 \\ 0 & \partial/\partial x_2 & 0 & \partial/\partial x_1 & \partial/\partial x_3 & 0 \\ 0 & 0 & \partial/\partial x_3 & 0 & \partial/\partial x_2 & \partial/\partial x_1 \end{bmatrix} \tag{4}$$

c is heat capacity and k is thermal conductivity relating to the thermal diffusion, both of them are considered as constants in this paper. Thermal dissipation ϕ is given as

$$\phi = \mu\left(\frac{\partial u_j}{\partial x_i} + \frac{\partial u_i}{\partial x_j}\right)\frac{\partial u_j}{\partial x_i} \tag{5}$$

μ is the non-Newtonian viscosity, the well-known power-law model [16–19] is considered in the present work, the segmented form of which is given as

$$\begin{cases} \mu = m\dot{\gamma}_0^{n-1}\mathrm{e}^{-\beta(T-T_{\mathrm{ref}})} & \text{if } (\dot{\gamma}\leqslant\dot{\gamma}_0) \\ \mu = m\dot{\gamma}^{n-1}\mathrm{e}^{-\beta(T-T_{\mathrm{ref}})} & \text{if } (\dot{\gamma}>\dot{\gamma}_0) \end{cases} \tag{6}$$

where the parameters m and n are called the consistency coefficient and the power law index, respectively, β is called the temperature dependency coefficient, T_{ref} is a reference temperature, constant $\dot{\gamma}_0 = 10^{-4}$ is adopted in this paper. $\dot{\gamma}$ is the rate of equivalent strain defined as

$$\dot{\gamma} = \sqrt{2D_{ij}D_{ji}} \quad D_{ij} = \frac{1}{2}\left(\frac{\partial u_j}{\partial x_i} + \frac{\partial u_i}{\partial x_j}\right) \tag{7}$$

where D_{ij} is the rate of strain tensor.

When thermal effects are ignored, Eq. (7) can be written as

$$\begin{cases} \mu = m\dot{\gamma}_0^{n-1} & \text{if } (\dot{\gamma}\leqslant\dot{\gamma}_0) \\ \mu = m\dot{\gamma}^{n-1} & \text{if } (\dot{\gamma}>\dot{\gamma}_0) \end{cases} \tag{8}$$

2.1. I-CNBS scheme for isothermal non-Newtonian fluid flow

Before proceeding with the split procedure of the fractional step scheme, we consider the discretization of Eq. (1) in time domain within a typical time sub-interval $[t_n, t_{n+1}]$ with $\Delta t = t_{n+1} - t_n$, which gives the form of the finite difference approximation (this form also can be classified as the single step θ method [19]) as

$$\frac{\rho}{\Delta t}(\mathbf{u}^{n+1} - \mathbf{u}^n) = \rho\mathbf{g} - (\rho\mathbf{u}\cdot\nabla\mathbf{u})^{n+\theta_2} + \left[\mathbf{S}^{\mathrm{T}}(\mu\mathbf{D}_0\mathbf{S})\mathbf{u}\right]^{n+\theta_1} - \nabla p^{n+\theta} \tag{9}$$

where θ_1, θ_2 and θ stand for time discretization choices of diffusive term, convective term, and pressure gradient term, respectively. To construct the fractional step scheme $\theta \neq 0$ for the pressure gradient term is required and $\theta = 0.5$ is usually taken for CN implicit scheme. Different choices for θ_1, $\theta_2 \in [0,1]$ corresponding to different schemes referred in the literature may be taken, i.e. $\theta_1 = \theta_2 = 0$ for

explicit scheme, $\theta_2 = 0$, $\theta_1 = 0.5$ for semi-implicit (CN) schemes and $0 < \theta_1$, $\theta_2 \leqslant 1$ for full-implicit forms. For second-order accuracy of the discretization in time domain $\theta_1 = \theta_2 = \theta = 0.5$ for CN scheme is adopted in this paper.

An auxiliary variable $\mathbf{u}^*$ is introduced in such a way that Eq. (9) is written in the form as below

$$\frac{\rho}{\Delta t}(\mathbf{u}^* - \mathbf{u}^n) = \rho\mathbf{g} - (\rho\mathbf{u}\cdot\nabla\mathbf{u})^{n+\theta_2} + \mathbf{S}^{\mathrm{T}}(\mu^{n+\theta_1}\mathbf{D}_0\mathbf{S}) \times [\theta_1(\mathbf{u}^* - \mathbf{u}^n) + \mathbf{u}^n] - \nabla p^n \tag{10}$$

$$\frac{\rho}{\Delta t}(\mathbf{u}^{n+1} - \mathbf{u}^*) = \mathbf{S}^{\mathrm{T}}(\mu^{n+\theta_1}\mathbf{D}_0\mathbf{S})\left[\theta_1(\mathbf{u}^{n+1} - \mathbf{u}^*)\right] - \theta\nabla\Delta p \tag{11}$$

Removing the $\mathbf{u}^*$ terms from the right-hand sides to the left-hand sides, Eqs. (10) and (11) can be written as

$$\left[\frac{\rho}{\Delta t}\mathbf{I}_3 - \theta_1\mathbf{S}^{\mathrm{T}}(\mu^{n+\theta_1}\mathbf{D}_0\mathbf{S})\right](\mathbf{u}^* - \mathbf{u}^n) = \rho\mathbf{g} + \mathbf{S}^{\mathrm{T}}(\mu^{n+\theta_1}\mathbf{D}_0\mathbf{S})\mathbf{u}^n - (\rho\mathbf{u}\cdot\nabla\mathbf{u})^{n+\theta_2} - \nabla p^n \tag{12}$$

$$\left[\frac{\rho}{\Delta t}\mathbf{I}_3 - \theta_1\mathbf{S}^{\mathrm{T}}(\mu^{n+\theta_1}\mathbf{D}_0\mathbf{S})\right](\mathbf{u}^{n+1} - \mathbf{u}^*) = -\theta\nabla\Delta p \tag{13}$$

Taking the divergence of the vector Eq. (13) and substituting the incompressibility condition (2) into Eq. (13) result in the Poisson equation for the pressure given as

$$\theta\nabla^2\Delta p = \frac{\rho}{\Delta t}\nabla\cdot\mathbf{u}^* + \theta_1\nabla\cdot\left\{\nabla\cdot[\mu^{n+\theta_1}\nabla(\mathbf{u}^{n+1} - \mathbf{u}^*)]\right\} = \frac{\rho}{\Delta t}\nabla\cdot\mathbf{u}^* + h(\Delta\mathbf{u}) \tag{14}$$

The term $\theta_1\mathbf{S}^{\mathrm{T}}(\mu^{n+\theta_1}\mathbf{D}_0\mathbf{S})(\mathbf{u}^{n+1} - \mathbf{u}^*)$ in Eq. (13) resulted from a consistent derivation is discarded in Eq. (14), which can be regarded as part of the approximation introduced and inherent to the split scheme. The reasons for discarding the term are twofold. On the one hand, the dropped term is the differential of the difference $(\mathbf{u}^{n+1} - \mathbf{u}^*)$ one-order higher than the first term at the right-hand side of Eq. (14). The justification of discarding the term may be expected and indeed it is validated by the numerical study [20,21] that omission of the term does not cause inaccuracy, instead enhances stability of the scheme. On the other hand, preservation of the term will induce severe difficulties in the numerical solutions of Eq. (14) for the pressure.

To fulfill the momentum conservation equation for incompressible flow in the implicit sense from the view of both convective and diffusive terms, an iterative procedure is introduced to construct the so-called I-CNBS scheme of the stabilized fractional step scheme based on Eqs. (12)–(14) as follows:

(1) Let $\mathbf{u}_0^{n+1} = \mathbf{u}^n$ and the number of iterations $i \Leftarrow 1$.
(2) Compute $\mathbf{u}_i^{n+\theta_1}$, $\mathbf{u}_i^{n+\theta_2}$ by $\mathbf{u}_i^{n+\theta_j} = (1-\theta_j)\mathbf{u}^n + \theta_j\mathbf{u}_{i-1}^{n+1}$ $(j = 1, 2)$ and compute $\mu^{n+\theta_1} = \mu(\mathbf{u}^{n+\theta_1})$ according to the constitutive equation at local points, then use $\mathbf{u}_i^{n+\theta_1}$, $\mathbf{u}_i^{n+\theta_2}$ and $\mu^{n+\theta_1}$ to solve for $\mathbf{u}_i^*$ by Eq. (12).
(3) Determine Δp_i by the solution of the Poisson equation (14) and obtain $p_i^{n+1} = p^n + \Delta p_i$.
(4) Solve Eq. (13) to determine $\mathbf{u}_i^{n+1}$ by using $\mathbf{u}_i^*$ and Δp_i.
(5) Check for convergence of the ith iteration, if $\|(\mathbf{Q}_i^{n+1} - \mathbf{Q}_{i-1}^{n+1})/\mathbf{Q}_{i-1}^{n+1}\|_\infty \leqslant \varepsilon$ $(\mathbf{Q} = \mathbf{u}, p)$, terminate the iteration loop, otherwise $i \Leftarrow i + 1$ and go to (2).

2.2. Characteristic based temporal discretization of the energy equation

The time discretization of Eq. (3) along the characteristic gives the form of the characteristic-Galerkin method as

$$\begin{aligned}\frac{\rho c}{\Delta t}(T^{n+1} - T^n) &= -\rho c u_j^{n+1/2}\frac{\partial T^n}{\partial x_j} + \frac{\Delta t}{2}\rho c\left(u_l^n\frac{\partial u_j^n}{\partial x_l}\frac{\partial T^n}{\partial x_j} + u_j^{n+1/2}u_k^{n+1/2}\frac{\partial^2 T^n}{\partial x_j\partial x_k}\right) \\ &\quad + k\frac{\partial^2 T^{n+\theta_3}}{\partial x_j\partial x_j} - (1-\theta_3)k\Delta t u_k^{n+1/2}\frac{\partial}{\partial x_k}\frac{\partial^2 T^n}{\partial x_j\partial x_j} \\ &\quad + \phi^{n+\theta_3} - (1-\theta_3)\Delta t u_k^{n+1/2}\frac{\partial}{\partial x_k}\phi^n + \mathrm{O}(\Delta t^2)\end{aligned} \tag{15}$$

$\theta_3 = 0.5$ is adopted in this paper. Eq. (15) can be further written in the matrix-vector form as

$$\begin{aligned}\left(\frac{\rho c}{\Delta t}\mathbf{I}_3 - \theta_3 k\nabla^2\right)(T^{n+1} - T^n) &= -\rho c\mathbf{u}^{n+1/2}\cdot\nabla T^n + k\nabla^2 T^n + \phi^{n+\theta_3} \\ &\quad + \frac{\Delta t}{2}\rho c\left[(\mathbf{u}^n\cdot\nabla\mathbf{u}^n)\cdot\nabla T^n + \mathbf{u}^{n+1/2}\cdot(\mathbf{u}^{n+1/2}\cdot\nabla^2 T^n)\right] \\ &\quad - (1-\theta_3)\Delta t k(\mathbf{u}^{n+1/2}\cdot\nabla)\nabla^2 T^n - (1-\theta_3)\Delta t(\mathbf{u}^{n+1/2}\cdot\nabla)\phi^n\end{aligned} \tag{16}$$

This is the form of the characteristic-Galerkin method that will be used in the following sections.

2.3. Spatial discretization

The fractional step algorithm performs time discretization before the spatial discretization. The primitive unknown variables u_i, p, T are spatially approximated using standard finite element shape functions $\mathbf{N}_u$, $\mathbf{N}_p$, $\mathbf{N}_T$ and expressed in terms of their nodal values $\bar{\mathbf{u}}_i, \bar{\mathbf{p}}, \bar{\mathbf{T}}$ as

$$u_i = \mathbf{N}_\mathbf{u}\bar{\mathbf{u}}_i, \quad p = \mathbf{N}_p\bar{\mathbf{p}}, \quad T = \mathbf{N}_T\bar{\mathbf{T}} \tag{17}$$

By using the standard Galerkin procedure, the weak forms of Eqs. (12)–(14) and (16) along with the weak forms of respective natural boundary conditions can be written as [6]

$$\left[\frac{\rho}{\Delta t}\mathbf{M} + \theta_1(\mathbf{K}_\mathbf{u})^{n+\theta_1} - \theta_1(\mathbf{K}_u^\Gamma)^{n+\theta_1}\right](\bar{\mathbf{u}}^* - \bar{\mathbf{u}}^n) = -(\mathbf{K}_\mathbf{u})^{n+\theta_1}\bar{\mathbf{u}}^n - \rho(\mathbf{C}\bar{\mathbf{u}})^{n+\theta_2} + \mathbf{L}^{\mathrm{T}}\bar{\mathbf{p}}^n + \rho\mathbf{M}\mathbf{g} + \mathbf{f}_s \tag{18}$$

$$\begin{aligned}\left(\frac{\rho c}{\Delta t}\mathbf{M}_T + \theta_3\mathbf{K}_T - \theta_3\mathbf{K}_T^\Gamma\right)(\bar{\mathbf{T}}^{n+1} - \bar{\mathbf{T}}^n) &= -\rho c\mathbf{C}_T\bar{\mathbf{T}}^n - \mathbf{K}_T\bar{\mathbf{T}}^n + \mathbf{\Phi} + \mathbf{f}_T \\ &\quad - \rho c\frac{\Delta t}{2}(\mathbf{C}_1 - \mathbf{C}_2)\bar{\mathbf{u}}^n + (1-\theta_3)\Delta t\mathbf{K}_{T2}\bar{\mathbf{u}}^n + (1-\theta_3)\Delta t\mathbf{\Phi}_2\end{aligned} \tag{19}$$

$$\theta \mathbf{K}_p \Delta\bar{\mathbf{p}} = -\frac{\rho}{\Delta t}\mathbf{L}\bar{u}^* + \mathbf{f}_p \tag{20}$$

$$\left[\frac{\rho}{\Delta t}\mathbf{M} + \theta_1(\mathbf{K}_\mathbf{u})^{n+\theta_1} - \theta_1(\mathbf{K}_u^\Gamma)^{n+\theta_1}\right](\bar{\mathbf{u}}^{n+1} - \bar{\mathbf{u}}^*) = \theta \mathbf{L}^{\mathrm{T}} \Delta\bar{\mathbf{p}} \tag{21}$$

which can be in turn used to solve for nodal values $\bar{\mathbf{u}}^*, \mathbf{T}^{n+1}, \Delta\bar{\mathbf{p}}, \bar{\mathbf{u}}^{n+1}$. It is noted that the terms integrated along the boundaries, generated due to integration by parts and associated with unknown nodal variables $\bar{\mathbf{u}}^*$, $\bar{\mathbf{u}}^{n+1}$ and $\overline{\mathbf{T}}^{n+1}$ are removed to the left-hand sides of Eqs. (18), (19) and (21), respectively.

With omission of the high order terms of both diffusion and dissipation, Eq. (19) can be simplified as

$$\left(\frac{\rho c}{\Delta t}\mathbf{M}_T + \theta_3 \mathbf{K}_T - \theta_3 \mathbf{K}_T^\Gamma\right)(\overline{\mathbf{T}}^{n+1} - \overline{\mathbf{T}}^n) = -\rho c \mathbf{C}_T \overline{\mathbf{T}}^n - \mathbf{K}_T \overline{\mathbf{T}}^n + \mathbf{\Phi} + \mathbf{f}_T - \rho c \frac{\Delta t}{2}(\mathbf{C}_1 - \mathbf{C}_2)\bar{\mathbf{u}}^n \tag{22}$$

2.4. I-CNBS–CG scheme for non-isothermal non-Newtonian fluid flow

An iterative scheme for incompressible non-isothermal non-Newtonian fluid flows abbreviated as I-CNBS–CG is constructed in this section. A staggered solution scheme is particularly designed to solve the velocity–pressure variables by using CNBS scheme for the momentum and the mass conservation equations and to solve the temperature variables by using CG method for the energy conservation equation. The iterative process is performed over both CNBS and CG solution procedures.

It is remarked that the staggered solution procedure of the proposed I-CNBS–CG scheme is particularly fit in the solution structure with the existing fractional step algorithm designed for isothermal N–S fluid flows. Eq. (22) derived by the characteristic-Galerkin (CG) method to solve for the nodal temperatures as the primary variables is simply inserted into the solution procedure of the fractional step algorithm for isothermal incompressible fluid flow derived by CNBS scheme.

The iterative procedure described in Section 2.1 is introduced to construct the stabilized fractional step scheme abbreviated as I-CNBS–CG in terms of Eqs. (18), (20), (21) and (22) as follows:

(1) Let $\bar{\mathbf{u}}_0^{n+1} = \bar{\mathbf{u}}^n$, $\overline{\mathbf{T}}_0^{n+1} = \overline{\mathbf{T}}^n$ and the number of iterations $i \Leftarrow 1$.
(2) Compute $\bar{\mathbf{u}}_i^{n+\theta_1}$, $\bar{\mathbf{u}}_i^{n+\theta_2}$, $\bar{\mathbf{u}}_i^{n+\theta_3}$, $\overline{\mathbf{T}}_i^{n+\theta_1}$, $\overline{\mathbf{T}}_i^{n+\theta_3}$ by $\overline{\mathbf{A}}_i^{n+\theta_x} = (1-\theta_x)\overline{\mathbf{A}}^n + \theta_x \overline{\mathbf{A}}_{i-1}^{n+1}$ $(\overline{\mathbf{A}} = \bar{\mathbf{u}}, \overline{\mathbf{T}};\ \ \theta_x = \theta_1, \theta_2, \theta_3)$ and compute $\mu^{n+\theta_1} = \mu(\mathbf{u}^{n+\theta_1}, T^{n+\theta_1})$, $\mu^{n+\theta_3} = \mu(\mathbf{u}^{n+\theta_3}, T^{n+\theta_3})$ according to the constitutive equation at local points, then use them to solve for $\bar{\mathbf{u}}^*$ and $\overline{\mathbf{T}}_i^{n+1}$ by Eqs. (18) and (22), respectively.
(3) Determine $\Delta\bar{\mathbf{p}}$ by the solution of the Poisson equation (20) and obtain $\bar{\mathbf{p}}^{n+1} = \bar{\mathbf{p}}^n + \Delta\bar{\mathbf{p}}$.
(4) Solve Eq. (21) to determine $\bar{\mathbf{u}}_i^{n+1}$ by using $\bar{\mathbf{u}}^*$ and $\Delta\bar{\mathbf{p}}$.
(5) Check for convergence of the ith iteration, if $\left\|(\overline{\mathbf{Q}}_i^{n+1} - \overline{\mathbf{Q}}_{\mathbf{i-1}}^{\mathbf{n+1}})/\overline{\mathbf{Q}}_{\mathbf{i-1}}^{\mathbf{n+1}}\right\|_\infty \leqslant \varepsilon(\overline{\mathbf{Q}} = \bar{\mathbf{u}}, \overline{\mathbf{T}}, \bar{\mathbf{p}})$, terminate the iteration loop, otherwise $i \Leftarrow i+1$ and go to (2).

It should be noted that it is convenient to solve Eq. (18) for $\bar{\mathbf{u}}^*$ and Eq. (22) for $\overline{\mathbf{T}}_i^{n+1}$ simultaneously since the two equations possess similar structures.

To demonstrate the performance of the presented I-CNBS–CG scheme in solving non-isothermal non-Newtonian fluid flow problems, we take a scheme to run the same example problems in parallel for the purpose of comparisons of numerical results. The scheme is assumed to form on the basis of existing CNBS scheme designed for isothermal incompressible flows and its extension to the non-isothermal case, i.e. the energy conservation equation is also discretized by using the CN method in time domain as bellow

$$\left(\frac{\rho c}{\Delta t}\mathbf{M}_T + \theta_3 \mathbf{K}_T - \theta_3 \mathbf{K}_T^\Gamma\right)(\overline{\mathbf{T}}^{n+1} - \overline{\mathbf{T}}^n) = -\rho c \mathbf{C}_T \overline{\mathbf{T}}^{n+\theta_3} - \mathbf{K}_T \overline{\mathbf{T}}^n + \Phi + \mathbf{f}_{T1} \tag{23}$$

The assumed solution scheme is also designed in the staggered strategy to solve the velocity–pressure variables and the temperature variables by means of CNBS and CN methods, respectively. To make the results obtained by the proposed I-CNBS–CG and the above assumed scheme comparable, the iterative procedure is also introduced into the assumed scheme abbreviated as I-CNBS–CN, in which the iterative procedure is just as same as that used for I-CNBS–CG except using Eq. (23) instead of Eq. (22).

3. Numerical results

3.1. Isothermal plane Poiseuille flow problem

The power-law model given in formula (8) is adopted to constitutively model the non-Newtonian behavior in this example. The geometry of the problem along with the 5×30 element mesh is shown in Fig. 1a and b. Non-equal order interpolation elements, i.e. T6P3 triangle elements with 6 noded quadratic interpolation for the velocities and 3 noded linear interpolation for the pressure are used in this example. No slip conditions are prescribed at the solid wall boundaries and $p = 0$ is prescribed at the exit of the mould cavity. The constant velocity components at the entry boundary are prescribed as

$$u_y = 0,$$
$$u_x(0, y) = \alpha \frac{n}{n+1}\left(\frac{1}{m}\right)^{1/n}\left[\left(\frac{Y_0}{2}\right)^{1+1/n} - \left|y - \frac{Y_0}{2}\right|^{1+1/n}\right] \tag{24}$$

where m and n are power-law parameters, Y_0 is the height of the cavity, α is the coefficient to normalize the fluid flux equal to unit at the entry. The transient solutions for the example can be regarded as a device to obtain the steady state solution. The theoretical solution for the pressure at the steady state of the Poiseuille flow problem is given by

$$p^T = \alpha^n (X_0 - x) \tag{25}$$

where X_0 is the length of the cavity.

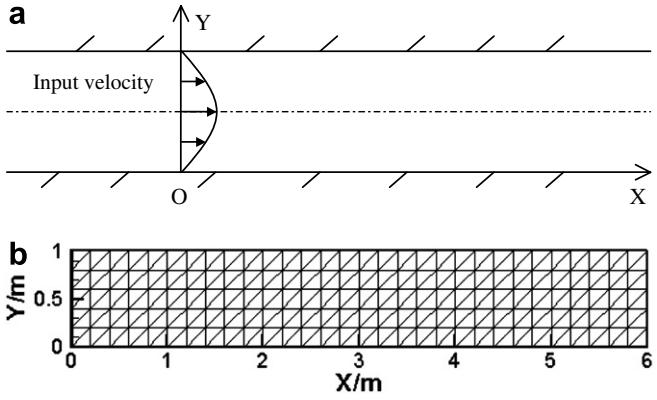

Fig. 1. The plane Poiseuille flow problem: (a) schematic diagram; (b) mesh plot.

In this example, the consistency coefficient m is taken as 100 Pa s, the problem is tested with three different values of power law index, i.e. $n = 0.8$, $n = 0.5$ and $n = 0.3$. It is understood that non-linear behavior of non-Newtonian fluid flows will become more prominent in this example at the zone near $Y = 0.5$ where the fluid viscosity varies along the Y-axis with high gradient, particularly as deviation of the value of power law index from unity increases as shown in Fig. 2. Indeed it is observed that as $n = 0.3$ is used the fluid viscosity varies along the Y-axis in a range of about 3.5 digital level. Consequently the maximum time step size allowed to be used for the example will decrease also with increasing deviation of the value of power law index from unity. Further, severe non-linearity will also bring a tough challenge to numerical methods to be used. The performances of the proposed scheme I-CNBS of the fractional step algorithm are compared with other two existing versions of the algorithm in accuracy and efficiency in carrying out this example. They are semi-implicit CNBS scheme mentioned above and the CBS [22,23] algorithm. Table 1 gives the maximum time step sizes allowed to be used for the different versions of the fractional step algorithm for numerical solutions of the problem with the three

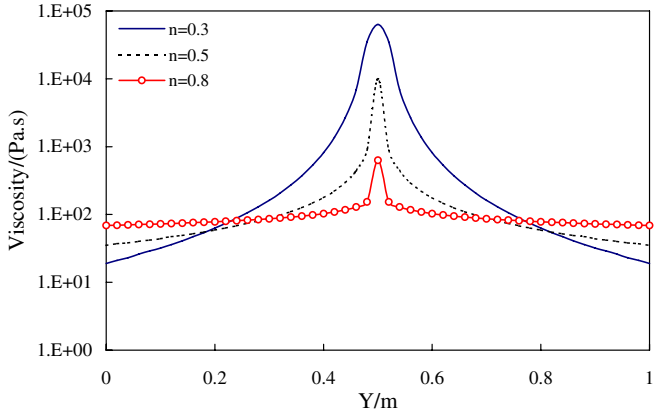

Fig. 2. Viscosity profiles for Poiseuille flow problem of power-law fluids.

Table 1
Comparisons of maximum time step sizes Δt_{max} (s) taken for different versions of the fractional step algorithm by using T6P3 elements in the solution for the plane Poiseuille flow problem with different power law indexes (in satisfaction of the convergence and the accuracy requirements)

	CBS	CNBS	I-CNBS
$n = 0.8$	0.01	1	1
$n = 0.5$	0.004	0.2	1
$n = 0.3$	Hard to converge	0.1	0.3

different values of power law index under acceptable convergence rate (number of time steps to achieve the steady state solution) and accuracy (the L^2 norm of the pressure error with respect to the analytical solution (25) is $\eta \leqslant 3\%$).

It is observed that the proposed iterative scheme I-CNBS performs much better in numerical solutions of the problem than the existing explicit algorithm CBS and semi-implicit scheme CNBS. The transient solutions converge to the steady state solution for CBS algorithm in the case of $n = 0.8$ with $\Delta t_{max} = 0.01$ s, which is much smaller than the value of Δt_{max} allowed to be used for the proposed I-CNBS, and what is worse, Δt_{max} for CBS algorithm gets further smaller with decreasing value of power law index until even no convergence is achieved in the case of $n = 0.3$, i.e. the transient solutions do not converge to the steady state solution after a huge number of time steps even with a very small time step size such as $\Delta t = 10^{-5}$ s. It is noted that the effects of the iterative procedure introduced into the scheme can be particularly demonstrated by a comparison of the maximum time step size required to CNBS and I-CNBS for the problems with moderate and low power law indices, i.e. the maximum time step sizes for the scheme I-CNBS five and three times of those for the scheme of CNBS for the cases of $n = 0.5$ and $n = 0.3$, respectively. (It should be noted that $\Delta t = 1$ s is considered as sufficient large time step size here although a time step size larger than $\Delta t = 1$ s may be used with acceptable convergence rate and accuracy, so do the other examples in this paper.)

The proposed I-CNBS scheme possesses the 2nd order convergence rate in temporal discretization as it is used to simulate the non-Newtonian flows. It can be indicated by checking the transient solutions at the "start-up" process, i.e. the unsteady state stage, of the same plane Poiseuille flow problem as described above. Particularly the problem is performed to calculate the pressure and velocity fields at $t = 2$ s with the use of different time step sizes. As there is no analytical solution available for the pressure at the unsteady state of the plane Poiseuille flow problem the finite element solutions with the refined 10×60 element mesh and the refined time step size 10^{-4} s are taken as the reference solutions. The relative error in pressure of the numerical solution obtained by I-CNBS scheme is measured by the L^2 norm defined as the normalized square of the pressure difference between nodal values obtained by the reference solution and the numerical solution using the 5×30 element mesh.

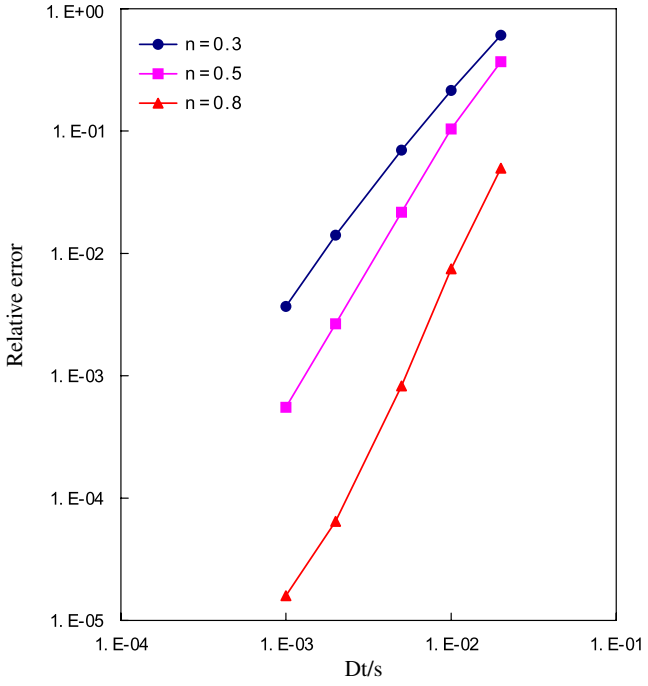

Fig. 3. Pressure error obtained by the proposed I-CNBS scheme at $t = 2$ s versus the time step.

The curves in Fig. 3, illustrate the relative errors in pressure which decrease with decreasing time step sizes for the different values of the power law index n used in the present simulation and demonstrate the second order accuracy for the pressure solution using the proposed I-CNBS scheme. It should be pointed out that the tested "start-up" process of the Poiseuille flow with the consideration of a specified discontinuity of the velocities prescribed at the entry of fluid flow, while null values of the pressure and velocity variables over the whole domain being specified, at $t = 0$ presents a tough task to challenge the performances of all numerical methods.

The performance, particularly the accuracy of the proposed I-CNBS scheme in solving the practical problems such as modeling of the injection molding process [6], in which there is no jump in the pressure and velocity fields with respect to time and space, will be greatly improved as compared with the accuracy of the tested case with $n = 0.3$ illustrated in Fig. 3.

3.2. Thermal 4:1 contraction problem

The numerical simulation of the flow in a 4:1 contraction problem represents a relatively difficult benchmark problem. Here, we examine the accuracy and convergence properties of the proposed I-CNBS–CG scheme for this problem by simulating the non-isothermal flow of power law fluids with temperature dependent viscosity.

By symmetry, only one half of the cavity of the 4:1 contraction problem is taken and discretized. Schematic statement of the problem with geometry and boundary

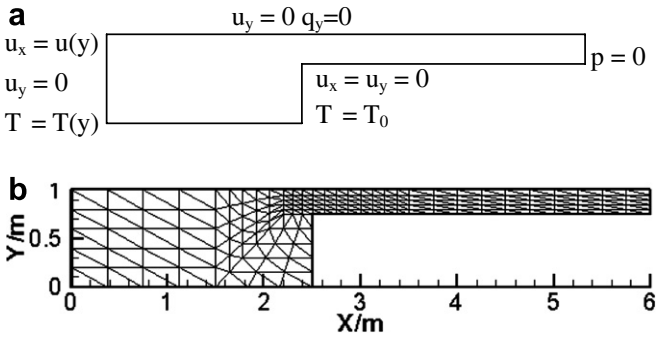

Fig. 4. The 4:1 contraction flow problem: (a) schematic diagram; (b) mesh plot.

conditions is depicted in Fig. 4a. The finite element mesh of T6P3 elements with the densities varying over the region is given in Fig. 4b (mesh1). To study the convergence of the proposed scheme in the spatial discretization, the other two refined meshes described by Table 2 are taken to perform the same example. The temperature T_0 along the three segments of the solid wall boundary is prescribed. The two cases associated with the two different values of T_0, i.e. $T_0 = 0$ °C and $T_0 = 100$ °C are particularly considered in the example. The temperature at the inlet is prescribed as $T(y) = T_{\text{entry}} = 50$ °C except at $y = 0$ where $T(y = 0) = T_0$ is prescribed. The boundary condition for the pressure is prescribed to be zero, i.e. $p = 0$ at the exit of the cavity of the 4:1 contraction problem. No slip conditions are prescribed at the solid wall boundaries. The velocity in the x-axis at the entry boundary is prescribed as

$$u_x(0, y) = \alpha y(2Y_0 - y) \tag{26}$$

where Y_0 is the height of the exit equal to unit, α is the coefficient to normalize the fluid flux equal to 0.04 m^2/s at the entry, i.e. $\alpha = 0.03$.

The thermal power-law model of viscosity is adopted in this example. Material parameters of the liquid are $m = 10^4$Pa s, $n = 0.5$, $T_{\text{ref}} = 50$ °C, $\beta = 0.01$ °C^{-1}, $\rho = 1000$ kg/m^3, $k = 1$ W/m K, respectively. The problem is particularly tested with the four thermal Peclet numbers, i.e. $Pe = 1,\ 10,\ 100,\ 1000$ corresponding to capacities $c = 0.05,\ 0.5,\ 5,\ 50$ Ws/kg K, respectively. $T_0 = 0$ °C and $T_0 = 100$ °C can be regarded as cooling and heating boundary conditions, respectively, in view of the inlet temperature $T_{\text{entry}} = 50$ °C. In the following, the numerical results obtained for the two cases of $T_0 = 0$ °C and $T_0 = 100$ °C will demonstrate the effects of the different thermal boundary conditions.

Table 2
Details of meshes employed

Mesh	Nodes	Elements	Typical element size between the lip and salient
Mesh1	731	330	0.15
Mesh2	877	398	0.125
Mesh3	1107	504	0.09375

Fig. 5 gives temperature profiles for the two cases with different values of thermal Peclet number equal to 1, 100, respectively, using mesh1. We may notice from these profiles the influence of increasing quantity of heat transferred due to convection, as compared with that of the quantity of heat transferred due to conduction, on the temperature distribution and the maximum of temperature in the flow field. For the case $T_0 = 0$ °C (the cooling wall case) the zones with low temperatures appear near the wall and diminish as Pe increases, whereas for the case $T_0 = 100$ °C (the heating wall case) the zones with low temperature appear near the inlet and expand with increasing value of Pe. We may also observed from Fig. 5a and c existence of the so-called local 'hot spots', which occur around the centerline at the contraction zone of the cavity and are the consequences of the viscous dissipation as a source of heat generation. As the value of Pe increases, the convection term, instead of viscous dissipation, dominants the heat transfer, these 'hot spots' tend to disappear as observed by other authors [24,25].

The curves of the axial pressure drop defined as $(p_{x=0} - p_{x=6})_{y=1}$ against Pe number for the three meshes using two different values of the prescribed temperature T_0 are given in Fig. 6. It is clear that the solutions for the two cases of T_0 converge consistently with high rate as mesh is refined. It is observed from Fig. 6 that the pressure drops for the case $T_0 = 0$ °C are much higher than those for the case $T_0 = 100$ °C, so that the external forces with higher strength normal to the inlet boundary are required to impose for the case $T_0 = 0$ °C in order to keep the velocities in the x-axis prescribed at the inlet. It is also noted that the pressure drops increase with increasing value of Pe for both cases. The viscosities of the fluid in this example are relatively high so that the diffusive term is a small quantity as compared with the dissipative term, so that the temperature at the local region with relatively high value of the dissipation term tends to go up. However, as the value of Pe increases significantly the heat convection will dominate the heat transfer instead of viscous dissipation that restrains the temperature to go up due to the dissipation effect and even results, in general, in lowering the temperature and consequently heightening the viscosity, and makes the fluid hard to flow, that explains why the pressure drop increases with increasing value of Pe.

Fig. 7 illustrates the streamlines of the thermal power-law fluid flow in the cavity of the 4:1 sudden contraction

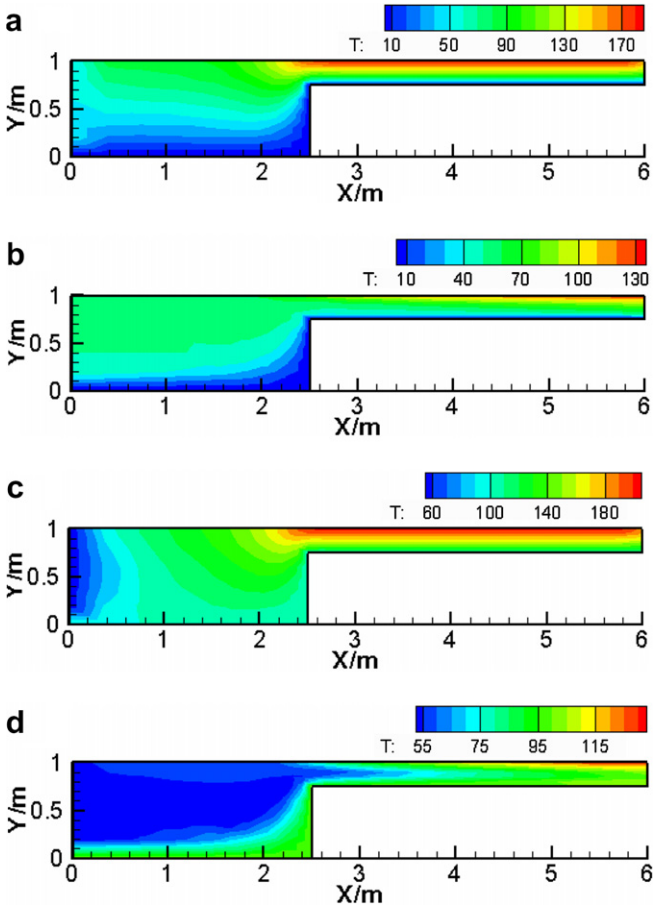

Fig. 5. Temperature profiles for the flow of a thermal power-law fluid in a 4:1 contraction problem. (a) $Pe = 1$, $T_0 = 0$ °C, $\Delta t = 0.05$ s; (b) $Pe = 100$, $T_0 = 0$ °C, $\Delta t = 0.1$ s; (c) $Pe = 1$, $T_0 = 100$ °C, $\Delta t = 0.1$ s; (d) $Pe = 100$, $T_0 = 100$ °C, $\Delta t = 0.1$ s.

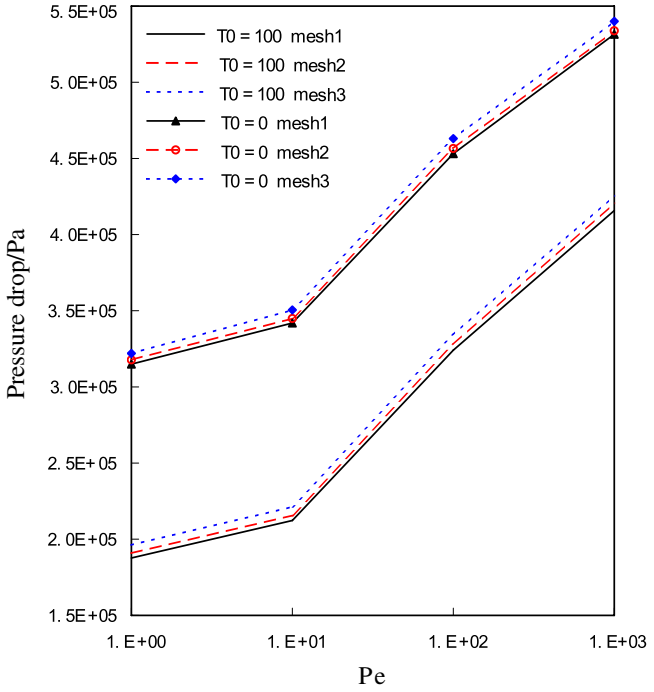

Fig. 6. Pressure drops calculated on different meshes for different Pe numbers of a thermal power-law fluid in a 4:1 contraction problem.

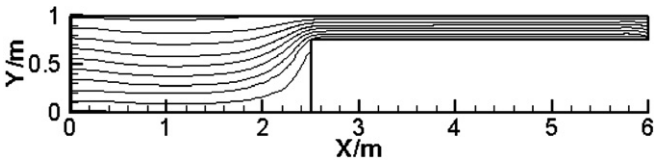

Fig. 7. Streamlines for the flow with a thermal power-law fluid in a 4:1 contraction problem ($Pe = 100$).

problem using mesh1. Even the resulting streamlines are obtained as $Pe = 100$ is used, the streamline plots resulted for the other cases of Pe, i.e. $Pe = 1$, 10, 1000 are essentially similar to those given in Fig. 7. It is also observed from Fig. 7 that there is no eddy that occurs in the down corner of the cavity, where the cross-section of the cavity is suddenly contract with the ratio 4:1. The pattern of streamlines for shear-thinning fluid observed in Fig. 7 is very similar to those published in the literature [24].

The numerical solutions obtained by using the assumed I-CNBS–CN scheme agree well with those obtained by the proposed I-CNBS–CG scheme only as thermal Peclet number is relatively small, for instance, $Pe \leqslant 10^2$. While for the case $Pe = 10^3$, the transient solutions converge to the steady state solution for the I-CNBS–CN scheme is only achieved as a time step size $\Delta t = 0.01$ s, 10 times smaller than that used for the I-CNBS–CG scheme, is used and after about 10 times of the time step number, i.e. 4876 steps, used for the I-CNBS–CG scheme are performed. Moreover, as the thermal Peclet number further increases, severe node-to-node oscillations will appear in the cavity and transient solutions fail to converge at all even with the small time step size $\Delta t = 0.01$ s.

4. Conclusions and discussion

An iterative stabilized CNBS–CG scheme for incompressible, non-isothermal, non-Newtonian fluid flows is presented in this paper.

The momentum and mass conservation equations are discretized by using the Crank–Nicolson implicit method based splitting (CNBS) scheme presented in [6], while the energy conservation equation is discretized by using the characteristic-Galerkin (CG) method. The iterative procedure is introduced to form the proposed I-CNBS–CG scheme, in which all the convective terms, diffusive terms and dissipative terms (for energy equation) are enforced to satisfy temporally semi-discretized equations in the implicit format. Numerical studies fulfilled in this paper indicate that

(1) Introduction of the iterative process into the fractional step algorithm, in general, enhances the critical time step size to ensure the stability of the scheme, particularly for the flow problems with moderate and high viscosities. As a consequence, the CPU time will be saved in a great deal as the time step size used increases. The simulation for a polymer injection molding example with a typical mould shown in Fig. 8 has demonstrated the superior performance of the proposed I-CNBS–CG scheme in computational efficiency over the existing explicit one. The CPU times required to perform the example for the two schemes are 218.5 s and more than 10^6 s, respectively, that prohibits, in fact, the use of the explicit algorithm in numerical simulations of practical polymer molding processes.

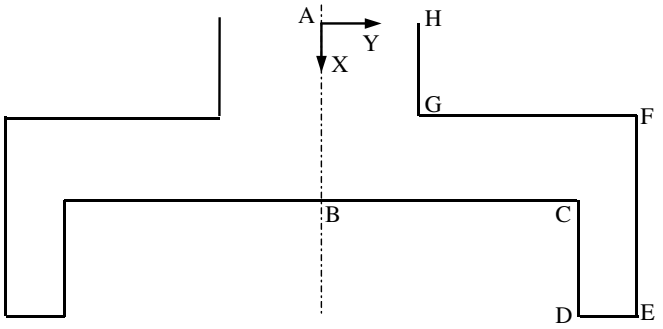

Fig. 8. Schematic diagram of a typical filling mould.

(2) The CG behaves better in the stability and convergence than the assumed CN in solving the energy equation, particularly for the flow problems with high thermal Peclet numbers.
(3) The proposed I-CNBS–CG scheme is suitable for modeling the fluid flows with moderate or high viscosity and low thermal conductivity, such as polymer solutions, melts, molten glass, etc.
(4) As mentioned above, the objective of this paper is to develop a scheme to simulate the fluid flows with high viscosity (low Re) and low thermal conductivity (high thermal Pe). The numerical study [6] has shown that for diffusion dominated problems, the iterative CN behaves better in the stability and allows to use time step sizes larger than or equal to that used for the iterative CG; while for convection dominated problems, the CG behaves better in convergence than the CN. It is known that both Re and thermal Pe reflect the ratio of convection term to diffusion term. That explains why we propose the I-CNBS–CG scheme for numerical solutions of incompressible non-isothermal non-Newtonian fluid flow.

Acknowledgements

The authors are pleased to acknowledge the support of this work by the National Natural Science Foundation of China through Contract/Grant numbers 10272027, 10590354 and 50278012 and the National Key Basic Research and Development Program (973 Program, No. 2002CB412709).

References

[1] A.J. Chorin, Numerical solution of the Navier–Stokes equations, Math. Comput. 22 (1968) 742–762.
[2] R. Temam, Sur 1' approximation de la solution des équations de Navier–Stokes par la méthode des pas fractionnaries II, Arch. Ration. Mech. Anal. 33 (1969) 377–385.
[3] S. Turek, A comparative study of time-stepping techniques for the incompressible Navier–Stokes equations: from fully implicit nonlinear schemes to semi-implicit projection methods, Int. J. Numer. Meth. Fluid 22 (1996) 987–1011.

[4] J.L. Guermond, L. Quartapelle, On stability and convergence of projection methods based on pressure Poisson equation, Int. J. Numer. Meth. Fluid 26 (1998) 1039–1053.
[5] R. Codina, Pressure stability in fractional step finite element methods for incompressible flows, J. Comput. Phys. 170 (2001) 112–140.
[6] X.K. Li, X.H. Han, An iterative stabilized fractional step algorithm for numerical solution of incompressible N–S equations, Int. J. Numer. Meth. Fluid 49 (2005) 395–416.
[7] X.K. Li, X.H. Han, M. Pastor, An iterative stabilized fractional step algorithm for finite element analysis in saturated soil dynamics, Comput. Meth. Appl. Mech. Eng. 192 (2003) 3845–3859.
[8] R. Codina, A. Folch, A stabilized finite element predictor-corrector scheme for the incompressible Navier–Stokes equations using a nodal-based implementation, Int. J. Numer. Meth. Fluid 44 (2004) 483–503.
[9] D.K. Garey, K.C. Wang, W.D. Joubert, Performance of iterative methods for Newtonian and generalized Newtonian flows, Int. J. Numer. Meth. Fluid 9 (1989) 127–150.
[10] M.N. Varma, A. Kannan, Enhanced food sterilization through inclination of the container walls and geometry modifications, Int. J. Heat Mass Tran. 48 (18) (2005) 3753–3762.
[11] C.W. Soh, Invariant solutions of the unidirectional flow of an electrically charged power-law non-Newtonian fluid over a flat plate in presence of a transverse magnetic field, Commun. Nonlinear Sci. Numer. Simulat. 10 (2005) 537–548.
[12] J. Chen, X.Y. Lu, L.X. Zhuang, W. Wang, Numerical analysis of the non-Newtonian blood flow in the nonplanar artery with bifurcation, J. Hydrodynam. 16 (3) (2004) 248–253.
[13] B.F. Fan, D.O. Kazmer, R. Nageri, An analytical non-Newtonian and nonisothermal viscous flow simulation, Poly-Plast. Technol. Eng. 45 (3) (2006) 429–438.
[14] M.H.R. Ghoreishy, V. Nassehi, Modeling the transient flow of rubber compounds in the dispersive section of an internal mixer with slip-stick boundary condition, Adv. Polym. Technol. 16 (1997) 45–68.
[15] X.H. Han, X.K. Li, An iterative stabilized fractional step algorithm for finite element analysis in high-viscosity fluid flows, Chi. J. Theor. Appl. Mech. 38 (1) (2006) 16–24 (in Chinese).
[16] R.B. Bird, J.M. Wiest, Constitutive equations for polymeric liquids, Ann. Rev. Fluid Mech. 27 (1995) 169–193.
[17] R.I. Tanner, Engineering rheology, Clarendon, Oxford, 1985, pp. 10–29.
[18] H.A. Barnes, J.F. Hutton, K. Walters, An introduction to rheology, Elsevier, New York, 1989, pp. 15–25.
[19] V. Nassehi, Practical Aspects of Finite Element Modelling of Polymer Processing, Wiley, West Sussex, 2001, pp. 4–8, 98–99.
[20] D.M. Hawken, H.R. Tomaddon-Jahromi, P. Townsend, A Taylor–Galerkin-based algorithm for viscous incompressible flow, Int. J. Numer. Meth. Fluid 10 (1990) 327–335.
[21] K.S. Sujatha, M.F. Webster, Modelling three-dimensional rotating flows in cylindrical-shaped vessels, Int. J. Numer. Meth. Fluid 43 (2003) 1067–1079.
[22] O.C. Zienkiewicz, P. Nithiarasu, R. Codina, M. Vazquez, P. Ortiz, The characteristic-based-split procedure: an efficient and accurate algorithm for fluid problems, Int. J. Numer. Meth. Fluid 31 (1999) 359–392.
[23] O.C. Zienkiewicz, R. Codina, A general algorithm for compressible and incompressible flow – part I: The split, characteristic-based scheme, Int. J. Numer. Meth. Fluid 20 (1995) 869–885.
[24] B.C. Bell, K.S. Surana, p-Version least squares finite element formulation for two-dimensional incompressible Newtonian and non-Newtonian non-isothermal fluid flow, Comput. Struct. 54 (1995) 83–96.
[25] C. Douglas, D. Roylance, Finite element flow analysis, North-Holland, New York, 1982.